JACS JOURNAL OF THE AMERICAN CHEMICAL SOCIETY

Article

Cite This: J. Am. Chem. Soc. 2019, 141, 5815−5823

pubs.acs.org/JACS

Characterization of a trans−trans Carbonic Acid−Fluoride Complex by Infrared Action Spectroscopy in Helium Nanodroplets

Daniel A. Thomas, Eike Mucha, Maike Lettow, Gerard Meijer, Mariana Rossi,* and Gert von Helden*

Fritz-Haber-Institut der Max-Planck-Gesellschaft, Faradayweg 4-6, 14195 Berlin, Germany

Supporting Information

ABSTRACT: The high Lewis basicity and small ionic radius of fluoride promote the formation of strong ionic hydrogen bonds in the complexation of fluoride with protic molecules. Herein, we report that carbonic acid, a thermodynamically disfavored species that is challenging to investigate experimentally, forms a complex with fluoride in the gas phase. Intriguingly, this complex is highly stable and is observed in abundance upon nanoelectrospray ionization of an aqueous sodium fluoride solution in the presence of gas-phase carbon dioxide. We characterize the structure and properties of the carbonic acid−fluoride complex, $F^-(H_2CO_3)$, and its deuterated isotopologue, $F^-(D_2CO_3)$, by helium nanodroplet infrared action spectroscopy in the photon energy range of 390−2800 cm^{-1}. The complex adopts a C_{2v} symmetry structure with the carbonic acid in a planar trans−trans conformation and both OH groups forming ionic hydrogen bonds with the fluoride. Substantial vibrational anharmonic effects are observed in the infrared spectra, most notably a strong blue shift of the symmetric hydrogen stretching fundamental relative to predictions from the harmonic approximation or vibrational second-order perturbation theory. Ab initio thermostated ring-polymer molecular dynamics simulations indicate that this blue shift originates from strong coupling between the hydrogen stretching and bending vibrations, resulting in an effective weakening of the OH···F^- ionic hydrogen bonds.

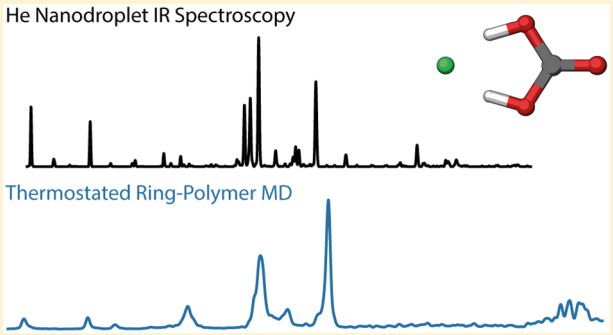

INTRODUCTION

The strong hydrogen bonds formed by halides are crucial in directing fundamental processes ranging from solvation to chemical reactivity. In aqueous halide solutions, the strength of the halide−water hydrogen bond strongly influences the local solvation structure and may also affect the solvent dynamics beyond the first solvation shell.[1−4] In choline halide-based deep eutectic solvents, strong halide hydrogen bonding interactions are the key structural motif leading to freezing -point suppression.[5−9] The fluoride anion, as a result of its small ionic radius and high Lewis basicity, forms particularly strong hydrogen bonds, leading to local solvation structures in protic solvents distinct from those of larger halides. For example, preferential hydrogen bonding to fluoride is observed in microsolvated water and methanol clusters,[1,10−12] and pronounced local ordering of water molecules is observed in bulk solution.[3] One intriguing and well-studied system is $F^-(H_2O)_2$, where, in contrast to larger halides, the favorable formation of hydrogen bonds with F^- disrupts the intermolecular aqueous hydrogen bonding network.[1] In addition, the strength of the fluoride−water hydrogen bonding interaction results in pronounced coupling between the vibrational modes associated with ionic hydrogen bond stretching, water rocking, and fluoride translation.[13]

Fluoride can also act as a potent nucleophile and has been used as a model reactant for studying nucleophilic substitution (S_N2) reactions.[14−17] Strong hydrogen bonding is likewise important in this context in which the complexation of fluoride with only a single water molecule significantly decreases the reaction rates.[14,17,18] In addition, the noncovalent capture of fluoride by hydrogen bond donor catalysts has been utilized to tune the enantioselectivity in nucleophilic substitution reactions.[19]

The nucleophilic properties of fluoride are also observed in its exothermic reaction with carbon dioxide to yield fluoroformate, FCO_2^-.[20,21] Recently, we described the generation of gas-phase fluoroformate by nanoelectrospray ionization of aqueous sodium fluoride in the presence of gas-phase carbon dioxide.[22] Herein, we report that the interaction of water, carbon dioxide, and fluoride in the electrospray process also results in the efficient production of a carbonic acid−fluoride complex.

The generation of a stable complex between carbonic acid and fluoride is highly intriguing. Carbonic acid is central to many chemical processes, yet it is thermodynamically unstable, undergoing decomposition to yield carbon dioxide and water.[23,24] Although the barrier to dissociation is large for an isolated carbonic acid molecule, the dissociation reaction is catalyzed by complexation with many abundant molecular

Received: December 19, 2018
Published: March 18, 2019

DOI: 10.1021/jacs.8b13542
J. Am. Chem. Soc. 2019, 141, 5815−5823

species, most notably water, ammonia, formic and acetic acid, and other carbonic acid molecules.[25−27] This catalytic decomposition renders the experimental characterization of carbonic acid extremely challenging. Thermolysis of ammonium bicarbonate gave the first experimental evidence for gas-phase H_2CO_3.[28] The first spectroscopic investigation of gas-phase carbonic acid was carried out in 2009 using microwave spectroscopy in a supersonic jet expansion,[29,30] and infrared spectroscopy of matrix-isolated carbonic acid was first reported in 2013.[31] Additionally, the structure of solid-phase carbonic acid was only unequivocally identified in 2014 after decades of debate.[23,32] In aqueous solution, the short lifetime of carbonic acid has also impeded experimental characterization,[24] with the first incontrovertible evidence for aqueous carbonic acid obtained by pump−probe spectroscopy in 2009.[33] More recently, the solvation structure of aqueous carbonic acid has been characterized by X-ray absorption spectroscopy,[34] and theoretical efforts have provided further insight into solvation and reactivity.[35−40]

The reaction dynamics of carbonic acid are highly sensitive to the local environment. For example, the water-catalyzed decomposition of carbonic acid occurs via a concerted proton-shuttle mechanism in microsolvated clusters but via an HCO_3^- intermediate in bulk solution,[36,38,40] and formation and decomposition mechanisms may differ at liquidlike and icelike surfaces.[41−43] There is also evidence that carbonic acid is formed catalytically on metal oxide surfaces.[44−47] However, little is known to date regarding the interaction of carbonic acid with ionic species other than protonated and deprotonated water. Thus, the complex examined herein provides a new opportunity to study the properties of this elusive molecule in an unexplored chemical environment.

This work explores the complex interplay of fluoride nucleophilic attack, strong hydrogen bonding, and proton transfer reactions in the fluoride−water−carbon dioxide system that yields the carbonic acid−fluoride complex. Infrared action spectroscopy of ions trapped in helium nanodroplets is employed to characterize this global minimum-energy structure. The low temperature of ca. 0.4 K provided by the helium nanodroplet environment enables the acquisition of highly resolved infrared spectra, which are matched to theoretical results from harmonic vibrational analysis, harmonic second-order perturbation theory, and ab initio thermostated ring-polymer molecular dynamics (TRPMD) to identify the experimentally observed structure and examine anharmonic effects in the vibrational spectrum. The chemical properties leading to the high stability of the carbonic acid−fluoride complex are discussed.

METHODS

Experimental Protocol. The experimental apparatus and methodology for helium nanodroplet ion infrared action spectroscopy have been described in several preceding publications,[48,49] and only specific parameters are provided herein. All samples and solvents were obtained from Sigma-Aldrich Merck (Darmstadt, Germany). Gas-phase ions were generated from a nanoelectrospray ionization (nESI) source with in-house-fabricated, Pd/Pt-coated borosilicate capillaries. Ions produced from nESI of a 1 mM aqueous solution of sodium fluoride were exposed to a flow of carbon dioxide introduced between the outer cone and inlet of the first vacuum stage of the mass spectrometer. Deuterium substitution of exchangeable hydrogens was carried out by passing the flow of carbon dioxide through a bubbler containing D_2O prior to introduction at the inlet.

Following ion transfer to vacuum, the ion of interest was isolated by utilizing a quadrupole mass filter and directed by means of a quadrupole ion bender to a hexapole ion trap, where a pulse of He buffer gas 2.0 s in length was utilized to collisionally cool and trap ions. To minimize background water pressure and reduce the reaction of the trapped species, the trap housing was cooled to ca. 95 K using a flow of liquid nitrogen. Additional details of the variable-temperature ion trap are given in the Supporting Information.

After ion trapping, a pump-down period of 1.5 s was implemented to reduce the pressure in the hexapole trap chamber. The ions were then captured in helium nanodroplets generated by a pulsed Even-Lavie valve[50] operating at a temperature of 23 K with a backing pressure of ca. 70 bar. Nanodroplets produced under these conditions were previously measured to contain on average 20 000 He atoms following ion pickup.[51] The nanodroplets with an entrained ion possessed sufficient kinetic energy to escape the potential well of the hexapole trap and travel to a time-of-flight (TOF) extraction region, where they were irradiated with infrared photons. The infrared beam was produced by the Fritz-Haber-Institut free-electron laser (FHI FEL), which generates a laser macropulse ca. 10 μs in length consisting of micropulses with a duration of ca. 5 ps and energy of ca. 10 μJ at a repetition rate of 1 GHz.[52] Resonant photon absorption followed by evaporative cooling resulted in a reduction in the helium nanodroplet size, and the sequential absorption of multiple photons within a laser macropulse yielded bare ions that were monitored by TOF mass spectrometry (MS). The integrated intensity of the ion of interest was utilized as an action signal to generate the infrared spectrum.

The ion signal detected by TOF MS was averaged over 25 laser pulses at a frequency of 10 Hz before the photon energy was changed and the hexapole trap was refilled with ions. A linear correction for laser power was applied to the intensity of each scan, and the presented spectra represent an average of two scans. As the output wavelength of the FHI FEL is variable over a limited range for a given electron energy,[52] the spectra were collected in separate experiments in three photon-energy ranges: 390−1050, 800−1900, and 1400−2800 cm^{-1}. The relative intensity of each partial spectrum was scaled on the basis of the intensity of spectral lines found in the overlapping measurement regions.

Ab Initio Calculations. Geometry optimization of candidate molecular structures was performed at the MP2/aug-cc-pVTZ level of theory[53−56] utilizing Gaussian 16.[57] Selected structures were also optimized at the CCSD(T)/aug-cc-pVTZ level of theory[58−60] with the CFOUR software package.[61,62] Zero-point energy corrections and relative free energies were determined within the harmonic approximation. Anharmonic corrections to the infrared spectra were calculated by utilizing the generalized second-order vibrational perturbation theory (GVPT2) method[63−65] at the MP2/aug-cc-pVTZ level of theory. A transition state search was performed using a quadratic synchronous transit (QST) approach,[66,67] and the identification of the correct transition state was confirmed by intrinsic reaction coordinate (IRC) calculations.[68,69]

For the ab initio TRPMD and ab initio molecular dynamics (AIMD) simulations, structures were first optimized by utilizing the B3LYP exchange-correlation density functional[70,71] and the pairwise van der Waals (vdW) correction[72] within the FHI-aims code[73] employing "tight" settings for basis set and numerical parameters. Harmonic infrared spectra were calculated using the method of finite differences. To approximate anharmonic nuclear quantum dynamics, ab initio TRPMD simulations[74] coupled to generalized Langevin equation thermostats were carried out as described previously.[75] Two simulations with 64 beads were run for $F^-(H_2CO_3)$, and 2 simulations with 48 beads were run for the deuterated isotopologue, each for 25 ps and at a temperature of 100 K after 5 ps of thermalization. Anharmonic infrared spectra were generated from the Fourier transform of the dipole autocorrelation function.

DOI: 10.1021/jacs.8b13542
J. Am. Chem. Soc. 2019, 141, 5815−5823

RESULTS AND DISCUSSION

Ions generated by nESI of a 1 mM aqueous solution of sodium fluoride were exposed to a flow of gas-phase carbon dioxide introduced at the atmospheric pressure inlet of a quadrupole time-of-flight mass spectrometer. The acquired mass spectrum shown in Figure 1 features three intense peaks at m/z 61, 63, and 81. The ion at m/z 61 is readily identified as hydrogen carbonate, HCO_3^-, which may be generated from dissolved carbonic acid in the sample or from the exothermic reaction of the hydroxide ion with carbon dioxide.[76] Similarly, the signal at m/z 63 is assigned to fluoroformate, produced by the reaction of fluoride with carbon dioxide described previously.[20,22] In contrast, the identity of the ion at m/z 81 is not immediately clear, although its substantial abundance in the mass spectrum suggests the formation of a stable and energetically favorable species. The m/z value nominally corresponds to a fluoroformate–water adduct, but the chemistry of the fluoride ion is likely complex, especially in the changing environment of an electrospray plume.[77] H/D exchange experiments conducted by introducing a flow of both gas-phase CO_2 and D_2O at the atmospheric pressure interface of the mass spectrometer showed that the ion at m/z 81 possesses two exchangeable hydrogens (Figure S1), and the composition was therefore nominally assigned as $[H_2CO_3F]^-$.

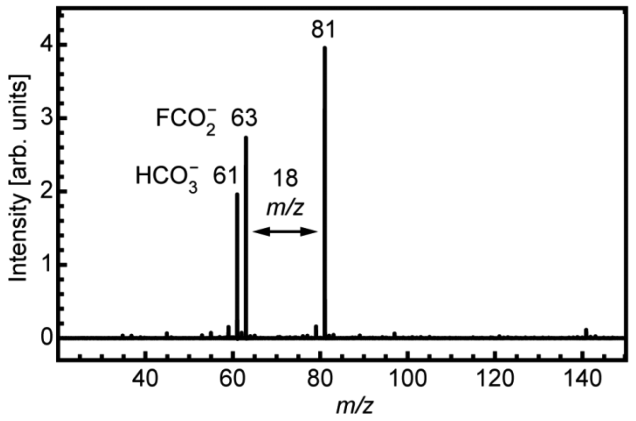

Figure 1. Mass spectrum obtained following nanoelectrospray ionization of 1 mM NaF in H_2O with a flow of gasesous CO_2 introduced at the atmospheric pressure interface into a quadrupole time-of-flight mass spectrometer. The spectrum features intense signals originating from three ions: hydrogen carbonate (HCO_3^-, m/z 61), fluoroformate (FCO_2^-, m/z 63), and an ion at m/z 81 assigned as $[H_2CO_3F]^-$.

MP2 calculations[53,54] with the aug-cc-pVTZ basis set[55] were utilized to investigate the relative free energies of putative structures of the $[H_2CO_3F]^-$ species. A partial reaction coordinate with notable local-energy-minimum structures is shown in Figure 2, and a full reaction coordinate detailing all identified structures is shown in Figure S2. The predicted global-minimum-energy structure, **1**, does not correspond to an ion–molecule complex between water and fluoroformate but rather to a complex between carbonic acid and fluoride. This complex features carbonic acid in a planar trans–trans conformation and belongs to the C_{2v} point group. Complexes comprising water and fluoroformate (**4** and **5**) are ca. 25 kJ mol^{-1} higher in free energy, and complexes comprising hydrogen fluoride and hydrogen carbonate (**2** and **3**) are ca. 8 kJ mol^{-1} higher in free energy.

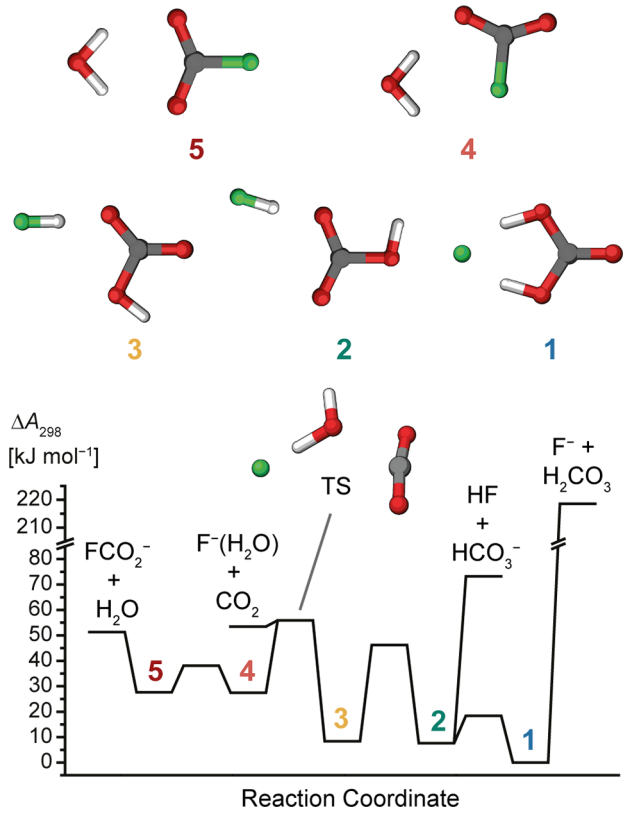

Figure 2. Partial reaction coordinate for the $[H_2CO_3F]^-$ species, showing the relative Helmholtz free energy at 298 K (ΔA_{298}, MP2/aug-cc-pVTZ) of five low-energy structures, the connecting transition states, and dissociation channels. The lowest-energy structure, **1**, comprises trans–trans carbonic acid complexed with fluoride, with conformations of hydrogen fluoride complexed with hydrogen carbonate (**2** and **3**) ca. 8 kJ mol^{-1} higher in free energy. Complexes comprising water and fluoroformate (**4** and **5**) are less stable by ca. 25 kJ mol^{-1}. A full reaction coordinate including all identified low-energy structures is shown in Figure S2.

The lowest-energy dissociative channel on the reaction coordinate yields fluoroformate and water, a process calculated to be approximately isoenergetic with the highest-energy transition state. Interestingly, this high-energy transition state, which connects water–fluoroformate structures (**4** and **5**) and hydrogen fluoride–hydrogen carbonate structures (**2** and **3**), strongly resembles a complex between $F^-(H_2O)$ and CO_2 (TS, Figure 2). Thus, the $F^-(H_2O)$ complex, which is energetically favored over desolvated F^- and thus likely formed in the electrospray process, can react with gas-phase CO_2 with a predicted barrier of less than 5 kJ mol^{-1} to enter the reaction coordinate shown in Figure 2. Microsolvated fluoride complexes featuring additional water molecules may also react via a similar transition state. Interestingly, this transition state strongly resembles that proposed for the formation of carbonic acid in aqueous solution, in which the nucleophilic attack of a water molecule at carbon dioxide is accompanied by proton transfer to yield HCO_3^- and H_3O^+.[40]

To probe the structure of the $[H_2CO_3F]^-$ species observed experimentally, the infrared spectrum was collected by utilizing action spectroscopy in helium nanodroplets. Figure 3 shows the experimental infrared spectrum of the $[H_2CO_3F]^-$ ion (top spectrum, black) as well as theoretical infrared spectra of candidate structures **1**–**5** (lower spectra, color) calculated at

DOI: 10.1021/jacs.8b13542
J. Am. Chem. Soc. 2019, 141, 5815–5823

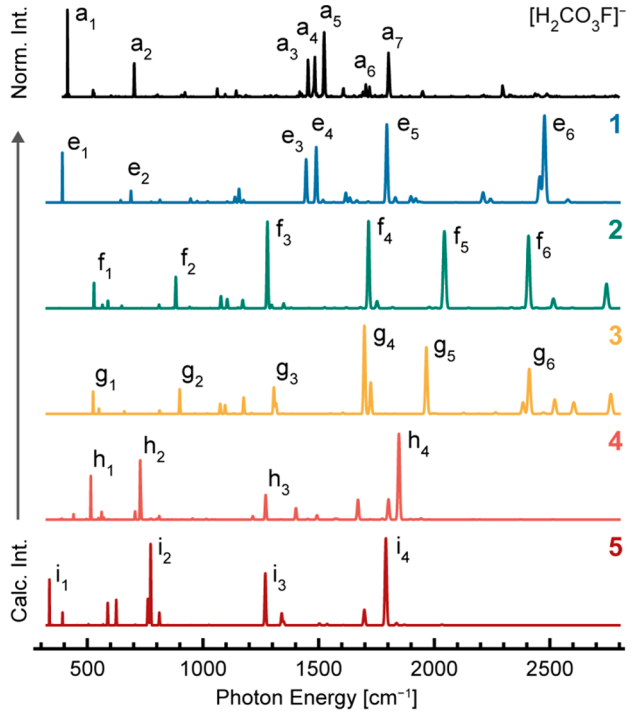

Figure 3. Experimental infrared spectrum of the $[H_2CO_3F]^-$ species compared to theoretical spectra of candidate structures. The experimental spectrum (black) was collected by ion infrared action spectroscopy in helium nanodroplets. Theoretical spectra for candidate structures **1**–**5** (Figure 2) were calculated at the MP2/aug-cc-pVTZ level of theory with anharmonic corrections from the GVPT2 method. The experimental spectrum below 2000 cm^{-1} matches best to the spectrum calculated for structure **1**. However, poor agreement between experiment and theory is observed for the hydrogen stretching vibrations appearing above 2000 cm^{-1}.

the MP2/aug-cc-pVTZ level of theory[53−56] with GVPT2 anharmonic corrections.[63−65] The spectral lines observed experimentally exhibit laser-bandwidth-limited full width at half-maximum (fwhm) values of ca. 0.5% of the incident photon energy, and the theoretical vibrational transition frequencies and intensities were convoluted with 0.5% fwhm Gaussian distributions to facilitate comparison to experiment.

The low-frequency region of the experimental spectrum of $[H_2CO_3F]^-$ is dominated by prominent bands at 414 and 703 cm^{-1} (bands a_1 and a_2, respectively), with weaker bands appearing between 800 and 1200 cm^{-1}. A more complex pattern of bands is observed at higher photon energies, with three closely spaced features at 1454, 1484, and 1524 cm^{-1} (bands a_3–a_5) as well as a single intense band at 1802 cm^{-1} (band a_7). No intense features are observed between 2000 and 2800 cm^{-1}.

The experimental spectrum is best replicated by the calculated spectrum of structure **1** (Figure 3, blue), which predicts an F^- displacement fundamental at 392 cm^{-1} (band e_1), a HO−C−OH bending fundamental at 689 cm^{-1} (band e_2), and a C═O stretch/O−H bend fundamental at 1795 cm^{-1} (band e_5). However, significant discrepancies between experiment and theory exist. Notably, the theoretical spectrum of **1** shows two rather than three lines between 1450 and 1550 cm^{-1}. Theory attributes these two lines to the fundamental of an in-plane OH bending mode (band e_4, symmetry species B_2) and a strongly shifted combination band of a low-frequency F^- translation mode and the asymmetric hydrogen stretching mode (band e_3, symmetry species A_1). In addition, the calculated spectrum of **1** predicts an intense symmetric hydrogen stretching fundamental at 2477 cm^{-1} (band e_6) that is not observed experimentally. Poor agreement is found between experiment and the predicted spectra of the hydrogen carbonate−hydrogen fluoride complexes (structures **2** and **3**). Similarly, the spectra of structures comprising fluoroformate and water (**4** and **5**) do not agree well with experiment, predicting no intense features near 1500 cm^{-1} and matching poorly at lower photon energies. It is possible that minor features in the experimental spectrum may arise from the population of higher-energy structural isomers, as kinetic trapping of structures with large barriers to rearrangement can occur during buffer gas cooling from room temperature to ca. 95 K in the ion trap[78] and, more notably, in cooling to ca. 0.4 K within the helium nanodroplet.[79,80]

The strong ionic hydrogen bonds formed in fluoride complexes can result in significant vibrational anharmonicity and mode coupling. To obtain an additional experimental probe of these effects, the infrared spectrum of the fully deuterated $[D_2CO_3F]^-$ system was also recorded, and the spectrum of $[D_2CO_3F]^-$ is compared to that of $[H_2CO_3F]^-$ in Figure 4. To provide a more straightforward comparison of

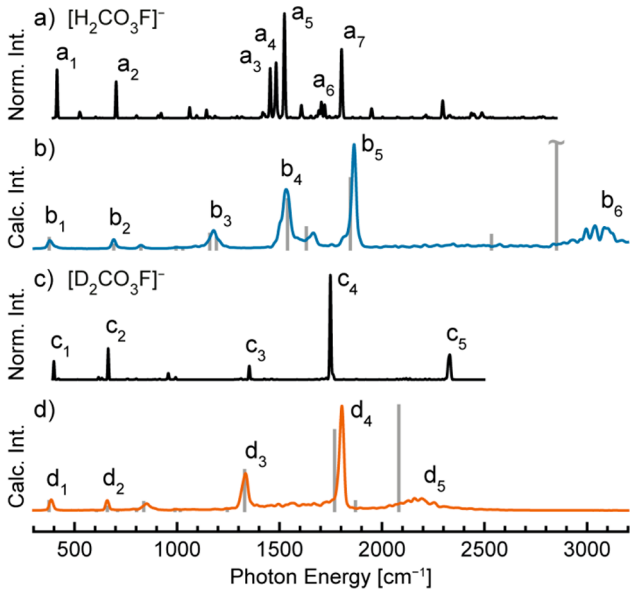

Figure 4. Experimental infrared spectrum of $[H_2CO_3F]^-$ (a) and its deuterated isotopologue $[D_2CO_3F]^-$ (c), compared to the theoretical spectra derived from TRPMD simulations at 100 K for $F^-(H_2CO_3)$ and $F^-(D_2CO_3)$ (b and d, respectively) with the B3LYP hybrid functional including vdW corrections. Calculated harmonic infrared spectra at the same level of theory are depicted with sticks in plots b and d. A Gaussian filter of σ = 2.5 cm^{-1} was applied to the experimental data for a more straightforward comparison of experimental and theoretical relative line intensities.

relative spectral line intensities, a Gaussian filter of σ = 2.5 cm^{-1} was applied to the experimental spectra. Although the low-energy bands of $[D_2CO_3F]^-$ (c_1 and c_2, Figure 4c) exhibit only slight red shifts from the corresponding bands of $[H_2CO_3F]^-$ (a_1 and a_2, Figure 4a), the spectra of the two isotopologues are profoundly different above 1200 cm^{-1}. Rather than the three bands near 1500 cm^{-1} and a slightly weaker band at 1802 cm^{-1} measured for $[H_2CO_3F]^-$, a single band at 1352 cm^{-1} (c_3) and an intense band centered at

DOI: 10.1021/jacs.8b13542
J. Am. Chem. Soc. 2019, 141, 5815−5823

1748 cm^{-1} (band c_4) are observed for $[D_2CO_3F]^-$. Additionally, a slightly broadened feature with maximum intensity at 2331 cm^{-1} (band c_5) is found at higher photon energies. Similar to $[H_2CO_3F]^-$, the experimental spectrum of $[D_2CO_3F]^-$ agrees best with the theoretical spectrum of structure **1** (Figure S3), but the intense symmetric OD stretching fundamental predicted at 1947 cm^{-1} (band j_5, Figure S3) is not observed experimentally.

For both $[H_2CO_3F]^-$ and $[D_2CO_3F]^-$, experimentally observed spectral lines can largely be replicated by theoretical spectra for structure **1** calculated with second-order perturbation corrections to the fundamental transitions of vibrational normal modes (i.e., GVPT2 corrections). However, the strong disagreement between experiment and theory in both the position and intensity of the symmetric hydrogen stretching fundamental suggests that an accurate description of acidic proton motion requires ab initio methods that extend beyond second-order perturbation corrections to the harmonic approximation. Therefore, thermostated ring-polymer molecular dynamics (TRPMD) simulations were utilized to investigate the properties of $F^-(H_2CO_3)$ and $F^-(D_2CO_3)$ (i.e., structure **1**) and to predict infrared spectra. The simulations utilized the B3LYP hybrid functional with vdW corrections and were carried out at a temperature of 100 K because it is challenging to conduct simulations at lower temperatures with this methodology. Harmonic spectra predicted by B3LYP calculations agree well with those obtained from CCSD(T) calculations (Tables S5 and S6), validating the use of this functional in the TRPMD simulations. Even though we do not expect this approximate methodology to quantitatively describe all features of the spectra due to the neglect of quantum coherence, we do expect it to yield a better approximation to anharmonic couplings than GVPT2.

Figure 4b,d shows the anharmonic infrared spectra obtained from the Fourier transform of the dipole autocorrelation function for $F^-(H_2CO_3)$ and $F^-(D_2CO_3)$, respectively. The corresponding harmonic infrared spectra are shown with a stick representation. Good agreement is observed between experimental and TRPMD anharmonic spectra, although some features such as the C═O stretch/O−H bend fundamental appear slightly blue-shifted (band a_7 vs band b_5 and band c_4 vs band d_4). It is not clear whether the triplet near 1480 cm^{-1} in the experimental spectrum of $[H_2CO_3F]^-$ (bands a_3−a_5) is fully replicated by TRPMD because band b_4 appears as a broad feature that encompasses at least two peaks but cannot be further deconvoluted. The experimental splitting may arise from a Fermi-type interaction that is not accurately captured at the current level of theory. Despite these differences, the broad agreement between experimental and TRPMD spectra enables a confident assignment of structure **1** as the principle species observed experimentally.

The largest difference between TRMPD and GVPT2 spectra is found in the predicted position and intensity of bands in the OH or OD stretching region. Whereas the GVPT2 method predicts a red shift relative to the harmonic approximation for the intense hydrogen or deuterium symmetric stretching fundamental, a strong blue shift is found by the TRPMD method (bands b_6 and d_5). All peaks are broadened with respect to experiment in the TRPMD spectra as a result of both the shortcomings of the theoretical method[74,75] and the higher simulation temperature. However, the symmetric hydrogen stretching bands for both $F^-(H_2CO_3)$ and $F^-(D_2CO_3)$ are more significantly broadened, likely as a result of strong coupling to overtones and combination bands of low-energy modes.[13]

To assess the role of nuclear quantum effects (NQEs) in the OH and OD stretching regions of the $F^-(H_2CO_3)$ and $F^-(D_2CO_3)$ systems, IR spectra were also calculated by ab initio molecular dynamics simulations with classical nuclei. As shown in Figure S4, the spectra obtained by this method yielded small differences from those obtained by TRPMD, most notably a further blue shift of the symmetric OH stretching band. This result demonstrates that the observed blue shift with respect to the harmonic prediction for both TRPMD and AIMD is largely the result of the strong anharmonicity of the vibrational potential energy surface. The role of NQEs is to slightly strengthen the H···F^- bond and weaken the OH bond, which is on average 0.01 Å longer in simulations employing TRPMD than in those utilizing AIMD. This behavior is consistent with previous studies on the role of NQEs in strong hydrogen bonds.[81]

The predicted band positions of the hydrogen stretching modes for $F^-(H_2CO_3)$ are outside of the experimentally accessible photon-energy range, but a comparison between experiment and theory is possible for $F^-(D_2CO_3)$. Experimentally, a slightly broadened feature is observed at 2331 cm^{-1} (band c_5, Figure 4c), whereas an extremely broad band near 2175 cm^{-1} is predicted by TRPMD simulations at 100 K (band d_5, Figure 4d). This discrepancy in band position may result in part from the difference between the simulated temperature of 100 K and the experimental temperature of ca. 0.4 K. A comparison of IR spectra of $F^-(D_2CO_3)$ obtained from AIMD simulations (classical nuclei) at 50 and 100 K shows a blue shift of band d_5 with decreasing temperature (Figure S5), supporting this explanation.

To yield further insight into the nature of acidic proton or deuteron motion, the vibrational density of states (VDOS) obtained from TRPMD simulations was projected onto the harmonic normal modes. Figure 5 shows the total calculated VDOS for $F^-(H_2CO_3)$ (Figure 5a) and $F^-(D_2CO_3)$ (Figure 5e) as well as the projection of the VDOS onto the harmonic normal modes associated with OH or OD bending (Figure 5b−c,f−g) and symmetric OH or OD stretching (Figure 5d,h). These results indicate that select in-plane and out-of-plane bending modes strongly couple to the symmetric OH or OD stretch. This intricate coupling can cause the observed blue shift with respect to the harmonic prediction by effectively making the OH stretching potential steeper than predicted in the harmonic approximation because the stretch is always accompanied by different bending motions that are also coupled to the H···F^- relative motion. A conclusive identification of the relevant atomic motion would require the application of a higher level of theory, for example, vibrational configuration interaction.[13,82,83]

The observed vibrational anharmonicity of the OH stretching modes in $F^-(H_2CO_3)$ results directly from the formation of two strong ionic hydrogen bonds. This structural motif is also responsible for the remarkable stability of the trans−trans carbonic acid−fluoride complex. Such double ionic hydrogen bonding has been reported previously in multiple systems with water as the hydrogen bond donor[84−86] but has not been observed for a carbonic acid complex. Indeed, in the absence of an anionic hydrogen bond acceptor, the trans−trans conformation is unfavorable relative to the cis−cis conformer in the gas phase (ΔH_0 = 42.3 kJ mol^{-1})[32] and in

DOI: 10.1021/jacs.8b13542
J. Am. Chem. Soc. 2019, 141, 5815−5823

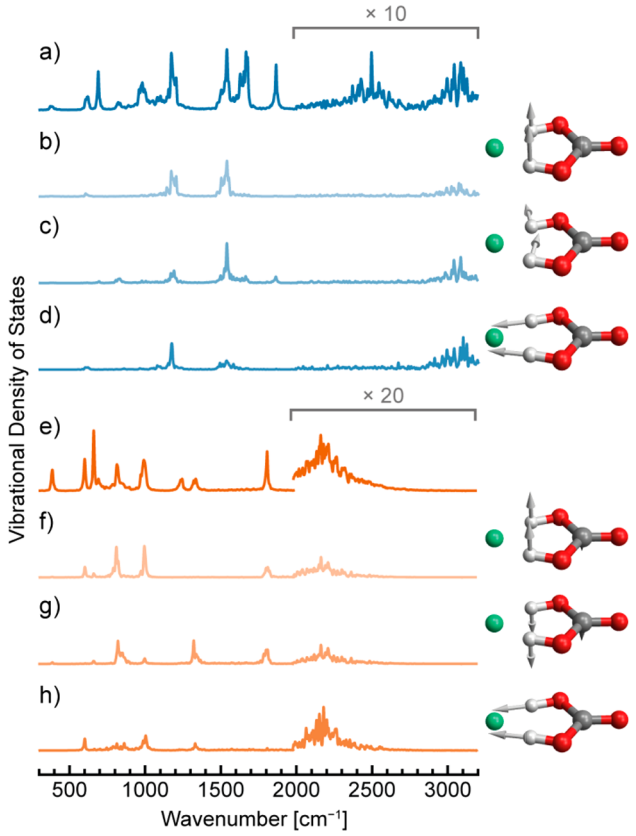

Figure 5. Vibrational density of states (DOS) derived from TRPMD calculations and their projection onto selected harmonic normal modes for $F^-(H_2CO_3)$ (a–d) and $F^-(D_2CO_3)$ (e–h). The total density of states is plotted in panels a and e, and the projections are shown in panels b–d and f–h along with the displacement vectors for the corresponding harmonic normal modes. Strong coupling is observed between the symmetric hydrogen stretching (d, h) and hydrogen bending (b–c, f–g) modes. The intensity in the range of 1900–3200 cm^{-1} is magnified as specified for all spectra, and the intensity in panels f–h is additionally magnified by a factor of 5 relative to panel e.

aqueous solution (ΔA_{315} = 26 kJ mol^{-1}).[38] The stabilization provided by the formation of the dual ionic hydrogen bonds is, however, sufficient to render the trans–trans conformer stable, with a calculated energy of 293 or 113 kJ mol^{-1} required to dissociate the complex to trans–trans carbonic acid and a free fluorine anion or hydrogen carbonate and hydrogen fluoride, respectively (0 K, MP2/aug-cc-pVTZ).

An assessment of the relationship between the anion proton affinity and ionic hydrogen bonding provides insight into the generality of the observed trans–trans carbonic acid binding motif. For single ionic hydrogen bonds, there is a well-established correlation between anion proton affinity and hydrogen bond strength, which is observed experimentally as a nearly linear correlation between the red shift of the hydrogen stretching modes and the anion proton affinity.[2,87] In the case of trans–trans carbonic acid, it is first interesting to observe that the double ionic hydrogen bond disfavors proton transfer from carbonic acid to the fluorine anion. The formation of HCO_3^- and HF is anticipated on the basis of experimental proton affinity measurements (1490 and 1555 kJ mol^{-1} for HCO_3^- and F^-, respectively)[88,89] and is in fact predicted for conformers featuring a single ionic hydrogen bond (structures **2**, **3**, and **6**). However, the weakening of the hydrogen bonds that would result from proton transfer disfavors this process for $F^-(H_2CO_3)$. Notably, the complexation of carbonic acid with a more basic anion counteracts the double ionic hydrogen bond stabilization, as is seen in the case of OH^-, where the higher proton affinity of the hydroxyl anion (1633 kJ mol^{-1})[89] results in proton transfer to yield low-energy $HCO_3^-(H_2O)$ structures.[90] In contrast, complexation with an anion of lower proton affinity weakens the double ionic hydrogen bond, offering less stabilization with respect to dissociation. Preliminary calculations on the $[H_2CO_3Cl]^-$ system (Cl^- proton affinity = 1395 kJ mol^{-1})[89] indicate that the $Cl^-(H_2CO_3)$ motif represents the global energy minimum but lies only 6.8 kJ mol^{-1} lower in free energy than dissociation to $Cl^-(H_2O)$ + CO_2 (Figure S8). We were also unable to observe the $[H_2CO_3Cl]^-$ ion experimentally. Thus, one can expect the stabilization of trans–trans carbonic acid by complexation with anions exhibiting a proton affinity in the range of ca. 1450 to 1600 kJ mol^{-1}.

CONCLUSIONS

In this work, we have investigated the intriguing reactions of fluoride, carbon dioxide, and water during the nanoelectrospray ionization process. The minimum-energy species on the investigated reaction surface is identified as a complex between carbonic acid and fluoride. The application of helium nanodroplet infrared spectroscopy to the study of this complex provides a detailed experimental characterization of its structure and properties. Although the spectroscopy is performed at a temperature of 0.4 K to obtain sufficient spectral resolution, both ab initio calculations and the high abundance of this ion in the mass spectrum suggest that $F^-(H_2CO_3)$ is the predominant species at room temperature. The exceptional stability of the carbonic acid–fluoride complex is rooted in the formation of two strong hydrogen bonds between fluoride and the hydroxyl groups of the carbonic acid. This double ionic hydrogen bonding motif yields strong anharmonic effects in the infrared spectrum that require high-level quantum chemical methods for accurate prediction.

ASSOCIATED CONTENT

Supporting Information

The Supporting Information is available free of charge on the ACS Publications website at DOI: 10.1021/jacs.8b13542.

Mass spectrum of nESI of 1 mM NaF with D_2O/CO_2 cone gas flow, expanded reaction coordinate of the $[H_2CO_3F]^-$ system, experimental vs theoretical spectra of $[D_2CO_3F]^-$ structures, additional IR spectra from AIMD and TRPMD, TRPMD free energy surfaces, experimental and theoretical spectral line positions, design of a variable-temperature ion trap, and calculated relative energies for the $[H_2CO_3Cl]^-$ system (PDF)

Tabulated experimental and TRPMD spectra and *xyz* coordinates and normal modes for theoretical structures (TXT)

AUTHOR INFORMATION

Corresponding Authors

*rossi@fhi-berlin.mpg.de

*helden@fhi-berlin.mpg.de

ORCID

Daniel A. Thomas: 0000-0001-9415-5991

DOI: 10.1021/jacs.8b13542
J. Am. Chem. Soc. 2019, 141, 5815–5823

Gerard Meijer: 0000-0001-9669-8340
Mariana Rossi: 0000-0002-3552-0677
Gert von Helden: 0000-0001-7611-8740

Notes

The authors declare no competing financial interest.

■ ACKNOWLEDGMENTS

The authors thank the employees of the mechanical workshop of the FHI for their diligence and expertise in the construction of a variable-temperature ion trap and Sandy Gewinner and Wieland Schöllkopf of the FHI FEL for laser operation. D.A.T. gratefully acknowledges the support of the Alexander von Humboldt Foundation.

■ REFERENCES

(1) Ayotte, P.; Nielsen, S. B.; Weddle, G. H.; Johnson, M. A.; Xantheas, S. S. Spectroscopic Observation of Ion-Induced Water Dimer Dissociation in the $X^-\cdot(H_2O)_2$ (X = F, Cl, Br, I) Clusters. *J. Phys. Chem. A* **1999**, *103*, 10665−10669.
(2) Robertson, W. H.; Johnson, M. A. Molecular Aspects of Halide Ion Hydration: The Cluster Approach. *Annu. Rev. Phys. Chem.* **2003**, *54*, 173−213.
(3) Migliorati, V.; Sessa, F.; Aquilanti, G.; D'Angelo, P. Unraveling Halide Hydration: A High Dilution Approach. *J. Chem. Phys.* **2014**, *141*, 044509.
(4) Schienbein, P.; Schwaab, G.; Forbert, H.; Havenith, M.; Marx, D. Correlations in the Solute−Solvent Dynamics Reach Beyond the First Hydration Shell of Ions. *J. Phys. Chem. Lett.* **2017**, *8*, 2373−2380.
(5) Abbott, A. P.; Capper, G.; Davies, D. L.; Rasheed, R. K.; Tambyrajah, V. Novel Solvent Properties of Choline Chloride/Urea Mixtures. *Chem. Commun.* **2003**, 70−71.
(6) Abbott, A. P.; Boothby, D.; Capper, G.; Davies, D. L.; Rasheed, R. K. Deep Eutectic Solvents Formed between Choline Chloride and Carboxylic Acids: Versatile Alternatives to Ionic Liquids. *J. Am. Chem. Soc.* **2004**, *126*, 9142−9147.
(7) Hammond, O. S.; Bowron, D. T.; Edler, K. J. Liquid Structure of the Choline Chloride-Urea Deep Eutectic Solvent (Reline) from Neutron Diffraction and Atomistic Modelling. *Green Chem.* **2016**, *18*, 2736−2744.
(8) Doherty, B.; Acevedo, O. OPLS Force Field for Choline Chloride-Based Deep Eutectic Solvents. *J. Phys. Chem. B* **2018**, *122*, 9982−9993.
(9) Fetisov, E. O.; Harwood, D. B.; Kuo, I. F. W.; Warrag, S. E. E.; Kroon, M. C.; Peters, C. J.; Siepmann, J. I. First-Principles Molecular Dynamics Study of a Deep Eutectic Solvent: Choline Chloride/Urea and Its Mixture with Water. *J. Phys. Chem. B* **2018**, *122*, 1245−1254.
(10) Corbett, C. A.; Martínez, T. J.; Lisy, J. M. Solvation of the Fluoride Anion by Methanol. *J. Phys. Chem. A* **2002**, *106*, 10015−10021.
(11) Robertson, W. H.; Diken, E. G.; Price, E. A.; Shin, J.-W.; Johnson, M. A. Spectroscopic Determination of the OH^- Solvation Shell in the $OH^-\cdot(H_2O)_n$ Clusters. *Science* **2003**, *299*, 1367−1372.
(12) Shi, R.; Wang, P.; Tang, L.; Huang, X.; Chen, Y.; Su, Y.; Zhao, J. Structures and Spectroscopic Properties of $F^-(H2O)_n$ with n = 1−10 Clusters from a Global Search Based On Density Functional Theory. *J. Phys. Chem. A* **2018**, *122*, 3413−3422.
(13) Kamarchik, E.; Bowman, J. M. Coupling of Low- and High-Frequency Vibrational Modes: Broadening in the Infrared Spectrum of $F^-(H_2O)_2$. *J. Phys. Chem. Lett.* **2013**, *4*, 2964−2969.
(14) O'Hair, R. A. J.; Davico, G. E.; Hacaloglu, J.; Dang, T. T.; DePuy, C. H.; Bierbaum, V. M. Measurements of Solvent and Secondary Kinetic Isotope Effects for the Gas-Phase S_N2 Reactions of Fluoride with Methyl Halides. *J. Am. Chem. Soc.* **1994**, *116*, 3609−3610.
(15) DePuy, C. H. Understanding Organic Gas-Phase Anion Molecule Reactions. *J. Org. Chem.* **2002**, *67*, 2393−2401.
(16) Garver, J. M.; Fang, Y.-r.; Eyet, N.; Villano, S. M.; Bierbaum, V. M.; Westaway, K. C. A Direct Comparison of Reactivity and Mechanism in the Gas Phase and in Solution. *J. Am. Chem. Soc.* **2010**, *132*, 3808−3814.
(17) Eyet, N.; Villano, S. M.; Bierbaum, V. M. Gas-Phase Reactions of Microsolvated Fluoride Ions: An Investigation of Different Solvents. *J. Phys. Chem. A* **2013**, *117*, 1136−1143.
(18) Zhang, J.; Yang, L.; Sheng, L. Electronic Structure Theory Study of the Microsolvated $F^-(H_2O)$ + CH_3I S_N2 Reaction. *J. Phys. Chem. A* **2016**, *120*, 3613−3622.
(19) Pupo, G.; Ibba, F.; Ascough, D. M. H.; Vicini, A. C.; Ricci, P.; Christensen, K. E.; Pfeifer, L.; Morphy, J. R.; Brown, J. M.; Paton, R. S.; Gouverneur, V. Asymmetric Nucleophilic Fluorination under Hydrogen Bonding Phase-Transfer Catalysis. *Science* **2018**, *360*, 638−642.
(20) Arnold, D. W.; Bradforth, S. E.; Kim, E. H.; Neumark, D. M. Study of Halogen−Carbon Dioxide Clusters and the Fluoroformyloxyl Radical by Photodetachment of $X^-(CO_2)$ (X = I,Cl,Br) and FCO_2^-. *J. Chem. Phys.* **1995**, *102*, 3493−3509.
(21) Zhang, X.; Gross, U.; Seppelt, K. Fluorocarbonate, $[FCO_2]^-$Preparation and Structure. *Angew. Chem., Int. Ed. Engl.* **1995**, *34*, 1858−1860.
(22) Thomas, D. A.; Mucha, E.; Gewinner, S.; Schöllkopf, W.; Meijer, G.; von Helden, G. Vibrational Spectroscopy of Fluoroformate, FCO_2^-Trapped in Helium Nanodroplets. *J. Phys. Chem. Lett.* **2018**, *9*, 2305−2310.
(23) Bucher, G.; Sander, W. Clarifying the Structure of Carbonic Acid. *Science* **2014**, *346*, 544−545.
(24) Loerting, T.; Bernard, J. Aqueous Carbonic Acid (H_2CO_3). *ChemPhysChem* **2010**, *11*, 2305−2309.
(25) de Marothy, S. A. Autocatalytic Decomposition of Carbonic Acid. *Int. J. Quantum Chem.* **2013**, *113*, 2306−2311.
(26) Ghoshal, S.; Hazra, M. K. New Mechanism for Autocatalytic Decomposition of H_2CO_3 in the Vapor Phase. *J. Phys. Chem. A* **2014**, *118*, 2385−2392.
(27) Ghoshal, S.; Hazra, M. K. $H_2CO_3 \rightarrow CO_2 + H_2O$ Decomposition in the Presence of H_2O, HCOOH, CH_3COOH, H_2SO_4 and HO_2 Radical: Instability of the Gas-Phase H_2CO_3 Molecule in the Troposphere and Lower Stratosphere. *RSC Adv.* **2015**, *5*, 17623−17635.
(28) Terlouw, J. K.; Lebrilla, C. B.; Schwarz, H. Thermolysis of NH_4HCO_3—A Simple Route to the Formation of Free Carbonic Acid (H_2CO_3) in the Gas Phase. *Angew. Chem., Int. Ed. Engl.* **1987**, *26*, 354−355.
(29) Mori, T.; Suma, K.; Sumiyoshi, Y.; Endo, Y. Spectroscopic Detection of Isolated Carbonic Acid. *J. Chem. Phys.* **2009**, *130*, 204308.
(30) Mori, T.; Suma, K.; Sumiyoshi, Y.; Endo, Y. Spectroscopic Detection of the Most Stable Carbonic Acid, *cis-cis* H_2CO_3. *J. Chem. Phys.* **2011**, *134*, 044319.
(31) Bernard, J.; Huber, R. G.; Liedl, K. R.; Grothe, H.; Loerting, T. Matrix Isolation Studies of Carbonic Acid—The Vapor Phase above the *β*-Polymorph. *J. Am. Chem. Soc.* **2013**, *135*, 7732−7737.
(32) Reisenauer, H. P.; Wagner, J. P.; Schreiner, P. R. Gas-Phase Preparation of Carbonic Acid and Its Monomethyl Ester. *Angew. Chem., Int. Ed.* **2014**, *53*, 11766−11771.
(33) Adamczyk, K.; Prémont-Schwarz, M.; Pines, D.; Pines, E.; Nibbering, E. T. J. Real-Time Observation of Carbonic Acid Formation in Aqueous Solution. *Science* **2009**, *326*, 1690−1694.
(34) Lam, R. K.; England, A. H.; Sheardy, A. T.; Shih, O.; Smith, J. W.; Rizzuto, A. M.; Prendergast, D.; Saykally, R. J. The Hydration Structure of Aqueous Carbonic acid from X-Ray Absorption Spectroscopy. *Chem. Phys. Lett.* **2014**, *614*, 282−286.
(35) Gallet, G. A.; Pietrucci, F.; Andreoni, W. Bridging Static and Dynamical Descriptions of Chemical Reactions: An Ab Initio Study of CO_2 Interacting with Water Molecules. *J. Chem. Theory Comput.* **2012**, *8*, 4029−4039.
(36) Galib, M.; Hanna, G. The Role of Hydrogen Bonding in the Decomposition of H_2CO_3 in Water: Mechanistic Insights from Ab

DOI: 10.1021/jacs.8b13542
J. Am. Chem. Soc. 2019, 141, 5815−5823

Initio Metadynamics Studies of Aqueous Clusters. *J. Phys. Chem. B* **2014**, *118*, 5983−5993.
(37) Liu, X.; Lu, X.; Wang, R.; Zhou, H. In Silico Calculation of Acidity Constants of Carbonic Acid Conformers. *J. Phys. Chem. A* **2010**, *114*, 12914−12917.
(38) Galib, M.; Hanna, G. Mechanistic Insights into the Dissociation and Decomposition of Carbonic Acid in Water via the Hydroxide Route: An Ab Initio Metadynamics Study. *J. Phys. Chem. B* **2011**, *115*, 15024−15035.
(39) Daschakraborty, S.; Kiefer, P. M.; Miller, Y.; Motro, Y.; Pines, D.; Pines, E.; Hynes, J. T. Reaction Mechanism for Direct Proton Transfer from Carbonic Acid to a Strong Base in Aqueous Solution I: Acid and Base Coordinate and Charge Dynamics. *J. Phys. Chem. B* **2016**, *120*, 2271−2280.
(40) Stirling, A.; Pápai, I. H_2CO_3 Forms via HCO_3^- in Water. *J. Phys. Chem. B* **2010**, *114*, 16854−16859.
(41) Galib, M.; Hanna, G. Molecular Dynamics Simulations Predict an Accelerated Dissociation of H_2CO_3 at the Air−Water Interface. *Phys. Chem. Chem. Phys.* **2014**, *16*, 25573−25582.
(42) Hirshberg, B.; Gerber, R. B. Formation of Carbonic Acid in Impact of CO_2 on Ice and Water. *J. Phys. Chem. Lett.* **2016**, *7*, 2905−2909.
(43) Miller, Q. R. S.; Ilton, E. S.; Qafoku, O.; Dixon, D. A.; Vasiliu, M.; Thompson, C. J.; Schaef, H. T.; Rosso, K. M.; Loring, J. S. Water Structure Controls Carbonic Acid Formation in Adsorbed Water Films. *J. Phys. Chem. Lett.* **2018**, *9*, 4988−4994.
(44) Taifan, W.; Boily, J.-F.; Baltrusaitis, J. Surface Chemistry of Carbon Dioxide Revisited. *Surf. Sci. Rep.* **2016**, *71*, 595−671.
(45) Henderson, M. A. Evidence for Bicarbonate Formation on Vacuum Annealed TiO_2(110) Resulting from a Precursor-Mediated Interaction Between CO_2 and H_2O. *Surf. Sci.* **1998**, *400*, 203−219.
(46) Baltrusaitis, J.; Grassian, V. H. Surface Reactions of Carbon Dioxide at the Adsorbed Water−Iron Oxide Interface. *J. Phys. Chem. B* **2005**, *109*, 12227−12230.
(47) Baltrusaitis, J.; Grassian, V. H. Carbonic Acid Formation from Reaction of Carbon Dioxide and Water Coordinated to $Al(OH)_3$A Quantum Chemical Study. *J. Phys. Chem. A* **2010**, *114*, 2350−2356.
(48) Mucha, E.; González Flórez, A. I.; Marianski, M.; Thomas, D. A.; Hoffmann, W.; Struwe, W. B.; Hahm, H. S.; Gewinner, S.; Schöllkopf, W.; Seeberger, P. H.; von Helden, G.; Pagel, K. Glycan Fingerprinting via Cold-Ion Infrared Spectroscopy. *Angew. Chem., Int. Ed.* **2017**, *56*, 11248−11251.
(49) González Flórez, A. I.; Mucha, E.; Ahn, D.-S.; Gewinner, S.; Schöllkopf, W.; Pagel, K.; von Helden, G. Charge-Induced Unzipping of Isolated Proteins to a Defined Secondary Structure. *Angew. Chem., Int. Ed.* **2016**, *55*, 3295−3299.
(50) Even, U. The Even-Lavie Valve as a Source for High Intensity Supersonic Beam. *EPJ. Technol. Instrum.* **2015**, *2*, 17.
(51) González Flórez, A. I. Biomolecular Ions in Superfluid Helium Nanodroplets. Ph.D. Thesis, Freie Universität Berlin, Berlin, 2015.
(52) Schöllkopf, W.; Gewinner, S.; Junkes, H.; Paarmann, A.; von Helden, G.; Bluem, H.; Todd, A. M. M. The new IR and THz FEL Facility at the Fritz Haber Institute in Berlin. *Proc. SPIE* **2015**, *9512*, 95121L.
(53) Møller, C.; Plesset, M. S. Note on an Approximation Treatment for Many-Electron Systems. *Phys. Rev.* **1934**, *46*, 618−622.
(54) Bartlett, R. J. Many-Body Perturbation Theory and Coupled Cluster Theory for Electron Correlation in Molecules. *Annu. Rev. Phys. Chem.* **1981**, *32*, 359−401.
(55) Kendall, R. A.; Dunning, T. H., Jr.; Harrison, R. J. Electron Affinities of the First Row Atoms Revisited. Systematic Basis Sets and Wave Functions. *J. Chem. Phys.* **1992**, *96*, 6796−6806.
(56) Woon, D. E.; Dunning, T. H., Jr. Gaussian Basis Sets for Use in Correlated Molecular Calculations. IV. Calculation of Static Electrical Response Properties. *J. Chem. Phys.* **1994**, *100*, 2975−2988.
(57) Frisch, M. J.; Trucks, G. W.; Schlegel, H. B.; Scuseria, G. E.; Robb, M. A.; Cheeseman, J. R.; Scalmani, G.; Barone, V.; Petersson, G. A.; Nakatsuji, H.; Li, X.; Caricato, M.; Marenich, A. V.; Bloino, J.; Janesko, B. G.; Gomperts, R.; Mennucci, B.; Hratchian, H. P.; Ortiz, J. V.; Izmaylov, A. F.; Sonnenberg, J. L.; Williams-Young, D.; Ding, F.; Lipparini, F.; Egidi, F.; Goings, J.; Peng, B.; Petrone, A.; Henderson, T.; Ranasinghe, D.; Zakrzewski, V. G.; Gao, J.; Rega, N.; Zheng, G.; Liang, W.; Hada, M.; Ehara, M.; Toyota, K.; Fukuda, R.; Hasegawa, J.; Ishida, M.; Nakajima, T.; Honda, Y.; Kitao, O.; Nakai, H.; Vreven, T.; Throssell, K.; Montgomery, J. A., Jr.; Peralta, J. E.; Ogliaro, F.; Bearpark, M. J.; Heyd, J. J.; Brothers, E. N.; Kudin, K. N.; Staroverov, V. N.; Keith, T. A.; Kobayashi, R.; Normand, J.; Raghavachari, K.; Rendell, A. P.; Burant, J. C.; Iyengar, S. S.; Tomasi, J.; Cossi, M.; Millam, J. M.; Klene, M.; Adamo, C.; Cammi, R.; Ochterski, J. W.; Martin, R. L.; Morokuma, K.; Farkas, O.; Foresman, J. B.; Fox, D. J. *Gaussian 16*, Revision A.03; Gaussian, Inc.: Wallingford, CT, 2016.
(58) Raghavachari, K.; Trucks, G. W.; Pople, J. A.; Head-Gordon, M. A Fifth-Order Perturbation Comparison of Electron Correlation Theories. *Chem. Phys. Lett.* **1989**, *157*, 479−483.
(59) Bartlett, R. J.; Watts, J. D.; Kucharski, S. A.; Noga, J. Non-Iterative Fifth-Order Triple and Quadruple Excitation Energy Corrections in Correlated Methods. *Chem. Phys. Lett.* **1990**, *165*, 513−522.
(60) Stanton, J. F. Why CCSD(T) Works: a Different Perspective. *Chem. Phys. Lett.* **1997**, *281*, 130−134.
(61) *CFOUR*; Coupled-Cluster techniques for Computational Chemistry, a quantum-chemical program package by Stanton, J. F., et al., with contributions from Auer, A. A., et al., PROPS by Taylor, P. R., et al., ABACUS by Helgaker, T., et al., and ECP routines by Mitin, A. V., et al. For the current version, see http://www.cfour.de.
(62) Harding, M. E.; Metzroth, T.; Gauss, J.; Auer, A. A. Parallel Calculation of CCSD and CCSD(T) Analytic First and Second Derivatives. *J. Chem. Theory Comput.* **2008**, *4*, 64−74.
(63) Barone, V. Anharmonic Vibrational Properties by a Fully Automated Second-Order Perturbative Approach. *J. Chem. Phys.* **2005**, *122*, 014108.
(64) Barone, V.; Bloino, J.; Guido, C. A.; Lipparini, F. A Fully Automated Implementation of VPT2 Infrared Intensities. *Chem. Phys. Lett.* **2010**, *496*, 157−161.
(65) Bloino, J.; Barone, V. A Second-Order Perturbation Theory Route to Vibrational Averages and Transition Properties of Molecules: General Formulation and Application to Infrared and Vibrational Circular Dichroism Spectroscopies. *J. Chem. Phys.* **2012**, *136*, 124108.
(66) Peng, C.; Bernhard Schlegel, H. Combining Synchronous Transit and Quasi-Newton Methods to Find Transition States. *Isr. J. Chem.* **1993**, *33*, 449−454.
(67) Peng, C.; Ayala, P. Y.; Schlegel, H. B.; Frisch, M. J. Using Redundant Internal Coordinates to Optimize Equilibrium Geometries and Transition States. *J. Comput. Chem.* **1996**, *17*, 49−56.
(68) Hratchian, H. P.; Schlegel, H. B. Accurate Reaction Paths using a Hessian based Predictor−Corrector Integrator. *J. Chem. Phys.* **2004**, *120*, 9918−9924.
(69) Hratchian, H. P.; Schlegel, H. B. Using Hessian Updating To Increase the Efficiency of a Hessian Based Predictor-Corrector Reaction Path Following Method. *J. Chem. Theory Comput.* **2005**, *1*, 61−69.
(70) Becke, A. D. Density Functional Thermochemistry. III. The Role of Exact Exchange. *J. Chem. Phys.* **1993**, *98*, 5648−5652.
(71) Stephens, P. J.; Devlin, F. J.; Chabalowski, C. F.; Frisch, M. J. Ab Initio Calculation of Vibrational Absorption and Circular Dichroism Spectra Using Density Functional Force Fields. *J. Phys. Chem.* **1994**, *98*, 11623−11627.
(72) Tkatchenko, A.; Scheffler, M. Accurate Molecular Van Der Waals Interactions from Ground-State Electron Density and Free-Atom Reference Data. *Phys. Rev. Lett.* **2009**, *102*, 073005.
(73) Blum, V.; Gehrke, R.; Hanke, F.; Havu, P.; Havu, V.; Ren, X.; Reuter, K.; Scheffler, M. Ab Initio Molecular Simulations with Numeric Atom-Centered Orbitals. *Comput. Phys. Commun.* **2009**, *180*, 2175−2196.
(74) Rossi, M.; Ceriotti, M.; Manolopoulos, D. E. How to Remove the Spurious Resonances from Ring Polymer Molecular Dynamics. *J. Chem. Phys.* **2014**, *140*, 234116.

DOI: 10.1021/jacs.8b13542
J. Am. Chem. Soc. 2019, 141, 5815−5823

(75) Rossi, M.; Kapil, V.; Ceriotti, M. Fine Tuning Classical and Quantum Molecular Dynamics using a Generalized Langevin Equation. *J. Chem. Phys.* **2018**, *148*, 102301.
(76) Torrent-Sucarrat, M.; Varandas, A. J. C. Carbon Dioxide Capture and Release by Anions with Solvent-Dependent Behaviour: A Theoretical Study. *Chem. - Eur. J.* **2016**, *22*, 14056−14063.
(77) Kebarle, P.; Verkerk, U. H. Electrospray: From Ions in Solution to Ions in the Gas Phase, What We Know Now. *Mass Spectrom. Rev.* **2009**, *28*, 898−917.
(78) Harrilal, C. P.; DeBlase, A. F.; Fischer, J. L.; Lawler, J. T.; McLuckey, S. A.; Zwier, T. S. Infrared Population Transfer Spectroscopy of Cryo-Cooled Ions: Quantitative Tests of the Effects of Collisional Cooling on the Room Temperature Conformer Populations. *J. Phys. Chem. A* **2018**, *122*, 2096−2107.
(79) Skvortsov, D. S.; Vilesov, A. F. Using He Droplets for Measurements of Interconversion Enthalpy of Conformers in 2-Chloroethanol. *J. Chem. Phys.* **2009**, *130*, 151101.
(80) Leavitt, C. M.; Moore, K. B.; Raston, P. L.; Agarwal, J.; Moody, G. H.; Shirley, C. C.; Schaefer, H. F.; Douberly, G. E. Liquid Hot NAGMA Cooled to 0.4 K: Benchmark Thermochemistry of a Gas-Phase Peptide. *J. Phys. Chem. A* **2014**, *118*, 9692−9700.
(81) Li, X.-Z.; Walker, B.; Michaelides, A. Quantum Nature of the Hydrogen Bond. *Proc. Natl. Acad. Sci. U. S. A.* **2011**, *108*, 6369−6373.
(82) Yu, Q.; Bowman, J. M.; Fortenberry, R. C.; Mancini, J. S.; Lee, T. J.; Crawford, T. D.; Klemperer, W.; Francisco, J. S. Structure, Anharmonic Vibrational Frequencies, and Intensities of $NNHNN^+$. *J. Phys. Chem. A* **2015**, *119*, 11623−11631.
(83) Qu, C.; Bowman, J. M. IR Spectra of (HCOOH)2 and (DCOOH)2: Experiment, VSCF/VCI, and Ab Initio Molecular Dynamics Calculations Using Full-Dimensional Potential and Dipole Moment Surfaces. *J. Phys. Chem. Lett.* **2018**, *9*, 2604−2610.
(84) Marcum, J. C.; Weber, J. M. Microhydration of Nitromethane Anions from Both a Solute and Solvent Perspective. *J. Phys. Chem. A* **2010**, *114*, 8933−8938.
(85) Robertson, W. H.; Price, E. A.; Weber, J. M.; Shin, J.-W.; Weddle, G. H.; Johnson, M. A. Infrared Signatures of a Water Molecule Attached to Triatomic Domains of Molecular Anions: Evolution of the H-bonding Configuration with Domain Length. *J. Phys. Chem. A* **2003**, *107*, 6527−6532.
(86) Heine, N.; Asmis, K. R. Cryogenic Ion Trap Vibrational Spectroscopy of Hydrogen-Bonded Clusters Relevant to Atmospheric Chemistry. *Int. Rev. Phys. Chem.* **2015**, *34*, 1−34.
(87) Roscioli, J. R.; Diken, E. G.; Johnson, M. A.; Horvath, S.; McCoy, A. B. Prying Apart a Water Molecule with Anionic H-Bonding: A Comparative Spectroscopic Study of the $X^-{\cdot}H_2O$ (X = OH, O, F, Cl, and Br) Binary Complexes in the 600−3800 cm^{-1} Region. *J. Phys. Chem. A* **2006**, *110*, 4943−4952.
(88) Squires, R. R. Gas-Phase Thermochemical Properties of the Bicarbonate and Bisulfite Ions. *Int. J. Mass Spectrom. Ion Processes* **1992**, *117*, 565−600.
(89) Bartmess, J. E. Negative Ion Energetics Data. In *NIST Chemistry WebBook, NIST Standard Reference Database Number 69*; Linstrom, P. J., Mallard, W. G., Eds.; National Institute of Standards and Technology: Gaithersburg, MD, 2018.
(90) Garand, E.; Wende, T.; Goebbert, D. J.; Bergmann, R.; Meijer, G.; Neumark, D. M.; Asmis, K. R. Infrared Spectroscopy of Hydrated Bicarbonate Anion Clusters: $HCO_3^-(H_2O)_{1-10}$. *J. Am. Chem. Soc.* **2010**, *132*, 849−856.

DOI: 10.1021/jacs.8b13542
J. Am. Chem. Soc. 2019, 141, 5815−5823